Journal of Systems Engineering and Electronics
Vol. 34, No. 3, June 2023, pp.783 – 797

Event-triggered model-free adaptive control for a class of surface vessels with time-delay and external disturbance via state observer

CHEN Hua[1,2,*], SHEN Chao[1], HUANG Jiahui[1], and CAO Yuhan[3]

1. College of Science, Hohai University, Nanjing 210098, China; 2. College of Mechanical and Electrical Engineering, Hohai University, Changzhou 213022, China; 3. Hohai-Lille College, Hohai University, Nanjing 211100, China

Abstract: This paper provides an improved model-free adaptive control (IMFAC) strategy for solving the surface vessel trajectory tracking issue with time delay and restricted disturbance. Firstly, the original nonlinear time-delay system is transformed into a structure consisting of an unknown residual term and a parameter term with control inputs using a local compact form dynamic linearization (local-CFDL). To take advantage of the resulting structure, use a discrete-time extended state observer (DESO) to estimate the unknown residual factor. Then, according to the study, the inclusion of a time delay has no effect on the linearization structure, and an improved control approach is provided, in which DESO is used to adjust for uncertainties. Furthermore, a DESO-based event-triggered model-free adaptive control (ET-DESO-MFAC) is established by designing event-triggered conditions to assure Lyapunov stability. Only when the system's indicator fulfills the provided event-triggered condition will the control input signal be updated; otherwise, the control input will stay the same as it is at the last trigger moment. A coordinate compensation approach is developed to reduce the steady-state inaccuracy of trajectory tracking. Finally, simulation experiments are used to assess the effectiveness of the proposed technique for trajectory tracking.

Keywords: surface vessels, event-triggered condition (ETC), discrete-time extended state observer (DESO), model-free adaptive control (MFAC), coordinate compensation.

DOI: 10.23919/JSEE.2023.000075

1. Introduction

Surface vessel (SV) has become more and more important in many marine applications, including monitoring systems, reconnaissance, search and rescue work, hydrographic survey, etc [1−4]. It frequently depends on precise trajectory tracking to be able to accomplish these functionalities. A control law is also required for SVs in order to track intended trajectory [5−7]. As a result, it is particularly important to design an excellent and widely applicable controller. However, SVs must track targets precisely and effectively in a variety of sea conditions for diverse application situations, and harsh sea conditions disturb the attitude of the SV. Meanwhile, control systems face many problems due to the large weight of the SV and the sensor reaction time [8]. Therefore, it is difficult to find an applicable controller. In many circumstances, time delays in systems cause the system's progress to be highly influenced by its previous state, resulting in an adverse effect on the quality of the control system [9]. Therefore, in the research of the SVs, the significance of time delay cannot be ignored. In addition, when the control system works on the sea surface, it will inevitably be affected by external factors such as gusts and waves, and these external disturbances may lead to instability [10,11]. Hence, the bounded disturbance to the SVs is also the focus of this paper.

Many sophisticated control approaches have been investigated to maintain the desired performance of vessel autopilot systems since the inception of modern control theory [12]. In [13], an adaptive heading controller was developed for vessels with unknown control coefficients. For vessel track-keeping, an adaptive fuzzy gain autopilot is investigated [14]. It should be emphasized that the control inputs in these results are updated with periodic sampling. In this case, the control signal needs to be continuously updated. Not only does it lead to excessive resource consumption but also frequent rudder action causes wear on the actuators. To overcome this problem, event-triggered control (ETC) is proposed, which is an efficient control method that can reduce the communica-

Manuscript received May 06, 2022.
*Corresponding author.
This work was supported by the Natural Science Foundation of Jiangsu Province (BK20201159).

tion burden while achieving similar system performance with less information transmission and low action time of actuators [15]. Reference [16] constructd a state observer and a new adaptive law based on the system output at the sampling moment. Then, ETCs were introduced, and a user-adjustable ETC was designed to determine the instant of event-triggering. For the nonlinear time-delay system with unmodeled dynamics, [17] studied an adaptive fuzzy control method using the command filtering method, and introduces a dynamic ETC mechanism to dynamically adjust the threshold parameters. This paper takes ETC into consideration. The coordinate compensation algorithm can eliminate the steady-state error and achieve better tracking effect. Reference [18] proposed a coordinate compensation algorithm for the flame cutting problem of steel grids. The results show that the algorithm improves the cutting trajectory to a certain extent and makes up for the incomplete cutting problem in the process of flame cutting of steel grids. In the process of finishing the solid tool flank by using a computer numerical control (CNC) tool grinder, a coordinate compensation algorithm is introduced, which effectively reduces the influence of grinding wheel wear, improves the stability of grinding quality, and prolongs the service life of the grinding wheel [19]. For the automatic parking system, in order to improve the coordinate tracking error of the desired trajectory, [20] proposed a model-free adaptive control (MFAC) scheme based on coordinate compensation and achieved good results.

Generally, exact mathematical or physical expression of the vessel is critical for the control law's design. In previous studies, model-based control methods have been proposed, including networked control, optimal control, and so on [21−23]. However, the models' descriptions are difficult in practice, making these model-based control approaches inappropriate for practical applications. Therefore, model-uncertainty problems began to catch researchers' eyes. For the trajectory tracking issue of underactuated vessels, [24] suggested an improved nonlinear control approach based on sliding mode control (SMC) theory. Furthermore, [25] offered a recursive sliding mode dynamic surface output feedback control based on neural network observer to estimate uncertainty. However, in practical applications, SMC is prone to chattering, and the neural network control approach requires a huge amount of calculation, resulting in the control system's lack of adaptability and practicability. Recently, data-driven control technology has been widely used in many fields [26]. The MFAC method, which is based on dynamic linearization, is one of the data-driven control methods. Its controller design is based only on the controlled object's input and output data and is not dependent on the controlled object's dynamic model [27,28]. The MFAC approach is currently used effectively in the domains of vessel control, spaceship control, robot attitude control, automatic parking systems, high-speed motor control, etc. [29−33]. Despite the widespread usage of the MFAC approach, the system's time delay is rarely considered throughout the application process. Therefore, this paper adds a time delay on the basis of the MFAC to enhance the applicability of this method. We consider not only the system's time delay, but also external disturbances in order to ensure that the SV can travel normally in the tough environment. In the context of a disturbed nonlinear system with uncertainty, the discrete-time extended state observer (DESO) has been proven to work well [34]. DESO can be used to estimate the unknown terms when studying the disturbed nonlinear discrete-time system with uncertainties. In addition, we incorporate an event-triggered mechanism to make the DESO-MFAC approach remain relevant in a network context with restricted bandwidth. This can not only save excessive resource consumption, but also solve the problem of actuator wear caused by frequent rudder control. Finally, the method of adding coordinate compensation algorithm to reduce the tracking error in the control process is widely used in trajectory tracking control.

This work presents and proves the bounded convergence of an improved MFAC approach for SV systems with time delay and bounded disturbance. Firstly, local compact form dynamic linearization (CFDL) is used to linearize nonlinear systems. Then, to estimate the system's uncertainty after linearization, the DESO is used. In addition, an ETC mechanism has been added to solve the problem of limited bandwidth and actuator wear in vessel control. Further, a coordinate compensation technique is used to minimize the steady-state inaccuracy of trajectory tracking. Finally, the efficiency of the suggested approach on trajectory tracking is validated using simulation tests. The main highlights of this paper are as follows:

(i) On the basis of DESO-MFAC method [35], an event trigger mechanism is introduced, and an event trigger condition that can make the system stable is designed. This can effectively reduce the usage of communication resources.

(ii) Different from the systems studied by [20,27,29,36], time-delay and disturbance are added to the SV system, and we demonstrate that the proposed algorithm can be adapted to this system. And a coordinate compensation algorithm is introduced to eliminate

the steady-state error of trajectory tracking.

(iii) The proposed method only utilizes the input and output data of the system and does not rely on any model information.

The structure of this document is as follows: The SV's dynamic model and discretization are presented in Section 2. The dynamic linearization approach is presented in Section 3. Section 4 introduces the enhanced control approach as well as event-triggered conditions, and Section 5 exhibits the proposed method's bounded convergence. In Section 6, coordinate compensation algorithm is introduced. Sections 7 offers simulations, and Section 8 summarizes this paper.

2. Problem statement

The dynamic model of a SV is the key to studying its motion state. The mathematical model of SVs is presented initially, before the design method. Then, use Euler's discretization method to discretize the proposed model. Finally, introduce the idea of trajectory tracking control in this paper.

By using Lagrangian mechanics, the dynamic model [37] can be stated as

$$\begin{cases} \dot{x} = u\cos\psi - v\sin\psi \\ \dot{y} = u\sin\psi + v\cos\psi \\ \dot{\psi} = \Lambda \end{cases}$$

where the coordinate of the SV model's center of gravity in the earth coordinate system is represented by (x,y), and the yaw angle of the SV is represented by ψ, while the forward, lateral, and yaw angular velocity of the SV are represented by (u,v,Λ). Fig. 1 depicts a simplified model of the SV.

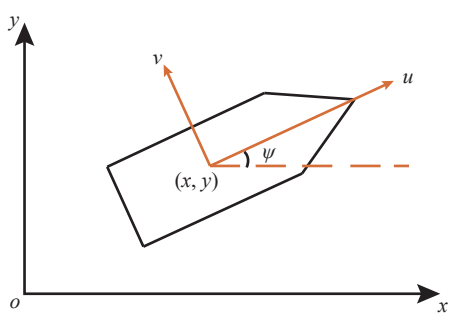

Fig. 1 SV model

In practical applications, the signals processed by the microprocessor are all digital signals, so the model needs to be discretized, but this approach will bring uncertainty to the system.

Based on Euler's discretization method [36], the model can be rewritten in the following way:

$$\begin{cases} \dfrac{x(j+1)-x(j)}{T} = u\cos(\psi(j)) - v\sin(\psi(j)) \\ \dfrac{y(j+1)-y(j)}{T} = u\sin(\psi(j)) + v\cos(\psi(j)) \\ \dfrac{\psi(j+1)-\psi(j)}{T} = \Lambda(j) + \Omega(j,\varsigma) \end{cases} \tag{1}$$

where T is sampling time.

The SV's position coordinates $(x(j),y(j))$ are connected to the yaw angle $\psi(j)$, the forward u, and the lateral v, according to the above-mentioned SV dynamic model (1). $\Omega(j,\varsigma)$ is the nonlinear term caused by internal or external factors of the SV, such as time delay, disturbance, etc. ς represents time delay of system.

In engineering applications, the forward u and the lateral v of the vessel are generally fixed when it comes to trajectory tracking problems such as low-speed docking and automatic driving at a constant speed. Therefore, when studying the trajectory tracking problem in this paper, let u, v be fixed.

The control goal of this paper is to make the actual trajectory $(x(j),y(j))$ of the vessel follow the desired trajectory $(x^*(j),y^*(j))$ by controlling the yaw angle $\psi(j)$.

3. Problem formation and local CFDL

3.1 Problem formation

The power plant of the SV is responsible for providing power to complete the forward and steering. Define the controllable power as Λ. The controllable power Λ and the yaw angle ψ of the SV are used as input and output (I/O) of controlled SV system, respectively. Due to sensor reaction time, SV mass, and other factors, the system's control input cannot be instantaneously stated as the system's output, and a time delay problem will arise. Meanwhile, complex sea surface conditions will have a certain impact on the output of the system. Consider a non-linear system with time delay in the input and disturbances

$$\psi(j+1) = g(\boldsymbol{\Psi}^{\mathrm{T}}(j),\boldsymbol{\Sigma}^{\mathrm{T}}(j-\varsigma),\boldsymbol{\Pi}^{\mathrm{T}}(j)) \tag{2}$$

where

$$\begin{cases} \boldsymbol{\Psi}^{\mathrm{T}}(j) = [\psi(j),\psi(j-1),\cdots,\psi(j-n_\psi)] \\ \boldsymbol{\Sigma}^{\mathrm{T}}(j-\varsigma) = [\Lambda(j-\varsigma),\Lambda(j-\varsigma-1),\cdots,\Lambda(j-\varsigma-n_\Lambda)] \\ \boldsymbol{\Pi}^{\mathrm{T}}(j) = [\pi(j),\pi(j-1),\cdots,\pi(j-n_\pi)] \end{cases}.$$

In (2), $\boldsymbol{\Psi}$, $\boldsymbol{\Sigma}$ represent the output and input of the control system. $g(\cdot)$ is a nonlinear function with initial condition $g(0,0,0)=0$. ς represents the time delay of the control system. n_ψ, n_Λ and n_π are system orders. $\boldsymbol{\Pi}$ is the bounded disturbance of the system that satisfies $\left|\sup\boldsymbol{\Pi}(j)\right| \leqslant b_\pi$.

Before employing the local CFDL approach to convert

the previously described nonlinear system into a linear one, we establish two assumptions.

Assumption 1 The partial derivatives of $g(\cdot)$ with respect to its components exist.

Assumption 2 The considered nonlinear function $g(\cdot)$ satisfies globally Lipschitz condition:

$$\begin{aligned}&|g(m_1(j_1),m_2(j_1),\cdots,m_P(j_1))-(m_2(j_2),m_1(j_2),\cdots,\\&m_P(j_2))|\leqslant K_1|m_1(j_1)-m_1(j_2)|+K_2|m_2(j_1)-\\&m_2(j_2)|+\cdots+K_P|m_P(j_1)-m_P(j_2)|\end{aligned}$$

where m_i are the terms of the function $g(\cdot)$ and $K_i>0$ is the Lipschitz constant, $i\in\{1,2,\cdots,P\}$; $P\in\mathbf{Z}^+$.

Remark 1 Assumption 1 is a common constraint condition for a class of nonlinear systems that can ensure the use of the mean value theorem throughout the linearization process. Assumption 2 is a quasi-linear condition, which can ensure that the change of the system output is limited by the change of the control input, so that it can be controlled within a certain range. In addition, many industrial processes can satisfy both assumptions, such as blast furnace ironmaking process [38] and the control of drum water level of circulating fluidized [39].

3.2 Model linearization

Satisfying Assumptions 1−2, the system in (2) can be written as:

$$\begin{aligned}&\Delta\psi(j+1)=g(\boldsymbol{\Psi}^{\mathrm{T}}(j),[\Lambda(j-\varsigma),\Lambda(j-\varsigma-1),\cdots,\\&\Lambda(j-\varsigma-n_\Lambda)],\boldsymbol{\Pi}^{\mathrm{T}}(j))+g(\boldsymbol{\Psi}^{\mathrm{T}}(j),[\Lambda(j-\varsigma-1),\\&\Lambda(j-\varsigma-1),\cdots,\Lambda(j-\varsigma-n_\Lambda)],\boldsymbol{\Pi}^{\mathrm{T}}(j))-g(\boldsymbol{\Psi}^{\mathrm{T}}(j),\\&[\Lambda(j-\varsigma-1),\Lambda(j-\varsigma-1),\cdots,\Lambda(j-\varsigma-n_\Lambda)],\\&\boldsymbol{\Pi}^{\mathrm{T}}(j))-g(\boldsymbol{\Psi}^{\mathrm{T}}(j-1),\boldsymbol{\Sigma}^{\mathrm{T}}(j-1),\boldsymbol{\Pi}^{\mathrm{T}}(j-1)).\end{aligned}$$

Using the median theorem, the above equation can be transformed into:

$$\begin{aligned}&\Delta\psi(j+1)=\frac{\partial g}{\partial\Lambda(j-\varsigma)}\Delta\Lambda(j-\varsigma)+\frac{\partial g}{\partial\psi(j)}\Delta\psi(j)+\\&\frac{\partial g}{\partial\psi(j-1)}\Delta\psi(j-1)+\cdots+\frac{\partial g}{\partial\psi(j-n_\psi)}\Delta\psi(j-n_\psi)+\\&\frac{\partial g}{\partial\Lambda(j-\varsigma-1)}\Delta\Lambda(j-\varsigma-1)+\frac{\partial g}{\partial\Lambda(j-\varsigma-2)}\Delta\Lambda(j-\varsigma-2)+\cdots+\\&\frac{\partial g}{\partial\Lambda(j-\varsigma-n_\Lambda)}\Delta\Lambda(j-\varsigma-n_\Lambda)+\frac{\partial g}{\partial\pi(j)}\Delta\pi(j)+\\&\frac{\partial g}{\partial\pi(j-1)}\Delta\pi(j-1)+\cdots+\frac{\partial g}{\partial\pi(j-n_\pi)}\Delta\pi(j-n_\pi),\end{aligned}$$

where

$$\begin{aligned}\Delta\psi(j)&=\psi(j)-\psi(j-1),\\\Delta\Lambda(j-\varsigma)&=\Lambda(j-\varsigma)-\Lambda(j-\varsigma-1),\\\Delta\pi(j)&=\pi(j)-\pi(j-1).\end{aligned}$$

The first-order partial derivative of $g(\cdot)$ with respect to control input $\Lambda(j-\varsigma)$ is denoted by $\partial g/\partial\Lambda(j-\varsigma)$, and one can guarantee the boundedness of $\left|\partial g/\partial\Lambda(j-\varsigma)\right|\leqslant L_{n_\psi+2}$, which is helpful for the following proofs, according to Assumption 2.

Let

$$\Xi(j-\varsigma)=\frac{\partial g}{\partial\Lambda(j-\varsigma)}$$

and

$$\begin{aligned}&\xi(j-\varsigma)=\frac{\partial g}{\partial\psi(j)}\Delta\psi(j)+\frac{\partial g}{\partial\psi(j-1)}\Delta\psi(j-1)+\cdots+\\&\frac{\partial g}{\partial\psi(j-n_\psi)}\Delta\psi(j-n_\psi)+\frac{\partial g}{\partial\Lambda(j-\varsigma-1)}\Delta\Lambda(j-\varsigma-1)+\\&\frac{\partial g}{\partial\Lambda(j-\varsigma-2)}\Delta\Lambda(j-\varsigma-2)+\cdots+\\&\frac{\partial g}{\partial\Lambda(j-\varsigma-n_\Lambda)}\Delta\Lambda(j-\varsigma-n_\Lambda)+\frac{\partial g}{\partial\pi(j)}\Delta\pi(j)+\\&\frac{\partial g}{\partial\pi(j-1)}\Delta\pi(j-1)+\cdots+\frac{\partial g}{\partial\pi(j-n_\pi)}\Delta\pi(j-n_\pi).\end{aligned}$$

Then, the system equation (2) can be rewritten as

$$\begin{cases}\Delta\psi(j+1)=\Xi(j-\varsigma)\Delta\Lambda(j-\varsigma)+\xi(j-\varsigma)\\\qquad\Updownarrow\\\Delta\psi(j+\varsigma+1)=\Xi(j)\Delta\Lambda(j)+\xi(j)\end{cases}\tag{3}$$

where $\xi(j)$ signifies the nonlinear uncertainty of the model in (3), and it will be calculated as a whole in the next controller design procedure.

Remark 2 Although (3) contains the nonlinear unknown term $\xi(j)$, this term can be regarded as a whole. In this paper, the discrete state vector observer is used to estimate the value of the whole, therefore, (3) can be said to be linear.

4. Controller design

4.1 DESO-based MFAC design

Consider the criterion function for $\Xi(j)$ [40]:

$$\begin{aligned}&J(\Xi(j))=|\psi(j+\varsigma)-\psi(j+\varsigma-1)-\\&\Xi(j)\Delta\Lambda(j-1)-\Xi(j-1)|^2+\eta|\Xi(j)-\Xi(j-1)|^2\end{aligned}$$

where $\eta>0$ is a weighting factor.

By finding the extreme value of the criterion function with respect to $\Xi(j)$, we can obtain

$$\begin{aligned}&\Xi(j)=\Xi(j-1)+\frac{\Delta\Lambda(j-1)}{\eta+|\Delta\Lambda(j-1)|^2}\cdot\\&(\Delta\psi(j+\varsigma)-\Xi(j-1)\Delta\Lambda(j-1)-\Xi(j-1)).\end{aligned}$$

Then, the estimation law is obtained as

$$\hat{\Xi}(j)=\hat{\Xi}(j-1)+\frac{\alpha_1\Delta\Lambda(j-1)}{\eta+|\Delta\Lambda(j-1)|^2}\cdot (\Delta\psi(j+\varsigma)-\hat{\Xi}(j-1)\Delta\Lambda(j-1)-\Xi(j-1)) \tag{4}$$

where $0<\alpha_1<2$ is a step factor and $\hat{\Xi}(j)$ is the estimated value of $\Xi(j)$.

Add a resetting algorithm to ensure that $\hat{\Xi}(j)$ can better estimate $\Xi(j)$

$$\hat{\Xi}(j)=\hat{\Xi}(0),$$
$$\left|\hat{\Xi}(j)\right|\leqslant\varepsilon;\quad \text{or } |\Delta\Lambda(j-1)|\leqslant\varepsilon;$$
$$\text{or } \operatorname{sign}(\hat{\Xi}(j))\neq\operatorname{sign}(\hat{\Xi}(0))$$

where ε is an arbitrarily small positive number.

Picking the appropriate value $\eta>0$, $0<\alpha_1<2$ can ensure bounded convergence of the estimation error of $\hat{\Xi}(j)$ to $\Xi(j)$. The bounded convergence will be proven in Theorem 1 in Section 5.

Remark 3 The resetting algorithm is to make $\hat{\Xi}(j)$ a better estimate of $\Xi(j)$. The use of the reset algorithm can ensure that during the application of the estimation algorithm in (4), the module of $\hat{\Xi}(j)$ and $\Delta\Lambda(j-1)$ will not become particularly small, and it can also ensure that the sign of $\hat{\Xi}(j)$ is always the same as $\Xi(j)$.

Remark 4 The derivation process of (4) is as follows:

$$J(\Xi(j))=|\psi(j+\varsigma)-\psi(j+\varsigma-1)-\Xi(j)\Delta\Lambda(j-1)-\Xi(j-1)|^2+\eta|\Xi(j)-\Xi(j-1)|^2.$$

For the above formula, find the partial derivative with respect to $\Xi(j)$ to get

$$\frac{\partial J}{\partial\Xi(j)}=-2\Delta\Lambda(j-1)(\psi(j+\varsigma)-\psi(j+\varsigma-1)-\Xi(j)\Delta\Lambda(j-1)-\Xi(j-1))+2\eta(\Xi(j)-\Xi(j-1)).$$

Let $\dfrac{\partial J}{\partial\Xi(j)}=0$,

$$\eta(\Xi(j)-\Xi(j-1))=\Delta\Lambda(j-1)(\psi(j+\varsigma)-\psi(j+\varsigma-1)-\Xi(j)\Delta\Lambda(j-1)-\Xi(j-1))=\Delta\Lambda(j-1)(\Delta\psi(j+\varsigma)-\Xi(j)\Delta\Lambda(j-1)+\Xi(j-1)\Delta\Lambda(j-1)-\Xi(j-1)\Delta\Lambda(j-1)-\Xi(j-1)).$$

Merge similar items to get

$$(\eta+\Delta\Lambda^2(j-1))(\Xi(j)-\Xi(j-1))=\Delta\Lambda(j-1)\cdot(\Delta\psi(j+\varsigma)-\Xi(j-1)\Delta\Lambda(j-1)-\Xi(j-1)).$$

Move items to get

$$\Xi(j)=\Xi(j-1)+\frac{\Delta\Lambda(j-1)}{\eta+|\Delta\Lambda(j-1)|^2}\cdot(\Delta\psi(j+\varsigma)-\Xi(j-1)\Delta\Lambda(j-1)-\Xi(j-1)),$$

$$\hat{\Xi}(j)=\hat{\Xi}(j-1)+\frac{\alpha_1\Delta\Lambda(j-1)}{\eta+|\Delta\Lambda(j-1)|^2}\cdot(\Delta\psi(j+\varsigma)-\hat{\Xi}(j-1)\Delta\Lambda(j-1)-\Xi(j-1)).$$

Let the desired output be $\psi^*(j)$, and define the tracking error as $e(j)=\psi^*(j)-\psi(j)$. Consider the criterion function for $\Lambda(j)$ [40] as follows:

$$J(\Lambda(j))=|\psi^*(j+\varsigma+1)-\psi(j+\varsigma+1)|^2+\lambda|\Lambda(j)-\Lambda(j-1)|^2 \tag{5}$$

where $\lambda>0$ is a weighting factor.

The control law can be derived by minimizing (5) in the following way:

$$\Lambda(j)=\Lambda(j-1)+\frac{\alpha_2\hat{\Xi}(j)}{\lambda+\left|\hat{\Xi}(j)\right|^2}\cdot(\psi^*(j+\varsigma+1)-\psi(j+\varsigma)-\xi(j)) \tag{6}$$

where $\alpha_2>0$ is a step factor.

Remark 5 Both α_1 and α_2 are step size factors of the control system, which can make the whole controller more universal. In practical applications, different values can be selected according to different application scenarios to make the proposed algorithm effective.

Remark 6 The derivation process of (6) is as follows:

$$J(\Lambda(j))=|\psi^*(j+\varsigma+1)-\psi(j+\varsigma+1)|^2+\lambda|\Lambda(j)-\Lambda(j-1)|^2=|\psi^*(j+\varsigma+1)-\psi(j+\varsigma)+\psi(j+\varsigma)-\psi(j+\varsigma+1)|^2+\lambda|\Lambda(j)-\Lambda(j-1)|^2=|\psi^*(j+\varsigma+1)-\psi(j+\varsigma)-\Xi(j)\Delta\Lambda(j)+\xi(j)|^2+\lambda|\Lambda(j)-\Lambda(j-1)|^2.$$

For the above formula, find the partial derivative with respect to $\Lambda(j)$ to get

$$\frac{\partial J}{\partial\Lambda(j)}=-2\Xi(j)(\psi^*(j+\varsigma+1)-\psi(j+\varsigma)-\Xi(j)\Delta\Lambda(j)+\xi(j))+2\lambda(\Lambda(j)-\Lambda(j-1)).$$

Let $\dfrac{\partial J}{\partial\Lambda(j)}=0$,

$$\lambda(\Lambda(j)-\Lambda(j-1))=\Xi(j)(\psi^*(j+\varsigma+1)-\psi(j+\varsigma)-\Xi(j)\Delta\Lambda(j)+\xi(j)).$$

Merge similar items to get

$$(\lambda+\Xi^2(j))(\Lambda(j)-\Lambda(j-1))=$$
$$\Xi(j)(\psi^*(j+\varsigma+1)-\psi(j+\varsigma)+\xi(j)).$$

Move items to get

$$\Lambda(j)=\Lambda(j-1)+\frac{\Xi(j)}{\lambda+|\Xi(j)|^2}\cdot$$
$$(\psi^*(j+\varsigma+1)-\psi(j+\varsigma)+\xi(j)),$$

$$\Lambda(j)=\Lambda(j-1)+\frac{\alpha_2\hat{\Xi}(j)}{\lambda+\left|\hat{\Xi}(j)\right|^2}\cdot$$
$$(\psi^*(j+\varsigma+1)-\psi(j+\varsigma)+\xi(j)).$$

Since $\xi(j)$ is unknown in both estimation law in (4) and control law in (6), to estimate $\xi(j)$, the extended state observer (ESO) technique [35] is used, as illustrated below.

Definite a vector

$$z(j)=[z_1(j),z_2(j-\varsigma)]^{\mathrm{T}}=[\psi(j),\xi(j-\varsigma)]^{\mathrm{T}},$$

which is equivalent to $z(j+\varsigma)=[\psi(j+\varsigma),\xi(j)]^{\mathrm{T}}$, and $\omega(j)=\xi(j+1)-\xi(j)$, The following equation can be represented according to (3):

$$\begin{cases}z(j+\varsigma+1)=\boldsymbol{A}_1z(j+\varsigma)+\boldsymbol{A}_2(j)\Delta\Lambda(j)+\boldsymbol{A}_3\omega(j)\\ \psi(j+\varsigma+1)=\boldsymbol{A}_4z(j+\varsigma+1)\end{cases}\tag{7}$$

where $\boldsymbol{A}_1=\begin{pmatrix}1&1\\0&1\end{pmatrix}$, $\boldsymbol{A}_2(j)=[\Xi(j),0]^{\mathrm{T}}$, $\boldsymbol{A}_3=[0,1]^{\mathrm{T}}$, $\boldsymbol{A}_4=[1,0]$.

For system (7), the discrete-time ESO is developed as follows:

$$\begin{cases}\hat{z}(j+\varsigma+1)=\boldsymbol{A}_1\hat{z}(j+\varsigma)+\hat{\boldsymbol{A}}_2(j)\Delta\Lambda(j)+\\ \qquad\boldsymbol{L}(\psi(j+\varsigma)-\hat{\psi}(j+\varsigma))\\ \hat{\psi}(j+\varsigma+1)=\boldsymbol{A}_4\hat{z}(j+\varsigma+1)\end{cases}\tag{8}$$

where $\boldsymbol{L}=[l_1,l_2]^{\mathrm{T}}$ is a gain vector; $\hat{\boldsymbol{A}}_2(j)=\left[\hat{\Xi}(j),0\right]^{\mathrm{T}}$. In addition, $\hat{z}(j+\varsigma)$ and $\hat{\psi}(j+\varsigma)$ denote the estimated value $z(j+\varsigma)$.

In conclusion, the entire control approach may be written as

$$\Lambda(j)=\Lambda(j-1)+\frac{\alpha_2\hat{\Xi}(j)}{\lambda+\left|\hat{\Xi}(j)\right|^2}\cdot$$
$$(\psi^*(j+\varsigma+1)-\psi(j+\varsigma)-\hat{z}_2(j)),\tag{9}$$

$$\hat{\Xi}(j)=\hat{\Xi}(j-1)+\frac{\alpha_1\Delta\Lambda(j-1)}{\eta+|\Delta\Lambda(j-1)|^2}\cdot$$
$$(\Delta\psi(j+\varsigma)-\hat{\Xi}(j-1)\Delta\Lambda(j-1)-\hat{z}_2(j-1)),\tag{10}$$

$$\hat{\Xi}(j)=\hat{\Xi}(0),\ \left|\hat{\Xi}(j)\right|\leqslant\varepsilon;$$
$$\text{or } |\Delta\Lambda(j-1)|\leqslant\varepsilon;$$
$$\text{or } \mathrm{sign}(\hat{\Xi}(j))\neq\mathrm{sign}(\hat{\Xi}(0)),\tag{11}$$

$$\begin{cases}\hat{z}(j+\varsigma+1)=\boldsymbol{A}_1\hat{z}(j+\varsigma)+\hat{\boldsymbol{A}}_2(j)\Delta\Lambda(j)+\\ \qquad\boldsymbol{L}(\psi(j+\varsigma)-\hat{\psi}(j+\varsigma))\\ \hat{\psi}(j+\varsigma+1)=\boldsymbol{A}_4\hat{z}(j+\varsigma+1)\end{cases}.\tag{12}$$

The control block diagram of the DESO-MFAC technique process is shown in Fig. 2.

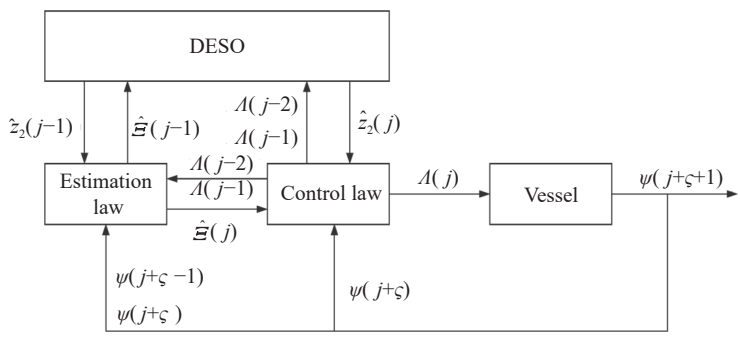

Fig. 2 Block diagram of DESO-MFAC control system

Obviously from the Fig. 2, the control principle of DESO-MFAC method is as follows:

Step 1 Initialize the estimated value of $\Xi(j-1)$ to be equal to $\hat{\Xi}(j-1)$. And initialize the estimated value of $z_2(j-1)$ to be equal to $\hat{z}_2(j-1)$.

Step 2 Using measurement input data $\Lambda(j-2)$, $\Lambda(j-1)$ and output data $\psi(j+\varsigma-1)$, $\psi(j+\varsigma)$ to calculate $\Xi(j)$ according to the estimation law (10) and resetting algorithm (11).

Step 3 Using measurement input data $\Lambda(j-2)$, $\Lambda(j-1)$ and the value of $\hat{\Xi}(j-1)$ to calculate $\hat{z}_2(j)$ according to DESO in (12).

Step 4 Using $\Xi(j)$ from Step 2 and $\hat{z}_2(j)$ from Step 3, and measurement output data $\psi(j+\varsigma)$, according to the expected output $\psi^*(j+\varsigma+1)$, control input $\Lambda(j)$ can be obtained via control law in (9).

Repeat the procedures above to get the system's output value closer and closer to the intended value.

4.2 Event-triggered mechanism

In modern SV' control, satellite communication or network communication is usually used to transmit data, which inevitably encounters the problem of limited communication bandwidth. An event-triggered mechanism is applied to deal with this problem.

The event-triggered time series is denoted as $\{j_\iota\}(\iota = 1, 2, \cdots)$ for clarity of the following description. Assume that the system's initial state is the event-triggered state. Only when the system's indicator fulfills the provided event trigger condition will the control input signal be updated; otherwise, the control input will stay the same as it was at the last trigger moment.

$$\Lambda(j) = \begin{cases} \Lambda(j_{\iota-1}) + \dfrac{\alpha_2 \hat{\Xi}(j)}{\lambda + \left|\hat{\Xi}(j)\right|^2} \cdot \\ \qquad (\psi^*(j+\varsigma+1) - \psi(j+\varsigma) - \hat{z}_2(j)), \ \ j = j_\iota \\ \Lambda(j_{\iota-1}), \ \ j \in (j_{\iota-1}, j_\iota) \end{cases}$$

Define event-triggered error $\sigma(j) = e(j_\iota) - e(j)$.

Let $H(j) = \left[(\alpha_2 \hat{\Xi}(j))/(\lambda + \left|\hat{\Xi}(j)\right|^2)\right]$. We design the event-triggered condition as

$$\sigma^2(j+\varsigma) > \frac{\kappa(j+\varsigma)}{2\Xi^2(j)H^2(j)} \tag{13}$$

where

$$\kappa(j+\varsigma) = e^2(j+\varsigma) - 4\left[(1 - \Xi(j)H(j)) \cdot \right.$$
$$\left.(\psi^*(j+\varsigma+1) - \psi(j+\varsigma) - \hat{z}_2(j))\right]^2.$$

If the event-triggered condition in (13) is fulfilled, then update the control input.

As a result, the DESO-based MFAC method with an event-triggered mechanism (ET-DESO-MFAC) is incorporated in the following way:

$$\hat{\Xi}(j) = \hat{\Xi}(j-1) + \frac{\alpha_1 \Delta\Lambda(j-1)}{\eta + |\Delta\Lambda(j-1)|^2} \cdot$$
$$(\Delta\psi(j+\varsigma) - \hat{\Xi}(j-1)\Delta\Lambda(j-1) - \hat{z}_2(j-1)), \tag{14}$$

$$\hat{\Xi}(j) = \hat{\Xi}(0), \ \left|\hat{\Xi}(j)\right| \leqslant \varepsilon;$$
$$\text{or } |\Delta\Lambda(j-1)| \leqslant \varepsilon;$$
$$\text{or } \operatorname{sign}(\hat{\Xi}(j)) \neq \operatorname{sign}(\hat{\Xi}(0)), \tag{15}$$

$$j = j_\iota, \quad \sigma^2(j+\varsigma) > \frac{\kappa(j+\varsigma)}{2\Xi^2(j)H^2(j)}, \tag{16}$$

$$\Lambda(j) = \begin{cases} \Lambda(j_{\iota-1}) + \dfrac{\alpha_2 \hat{\Xi}(j)}{\lambda + \left|\hat{\Xi}(j)\right|^2} \cdot \\ \qquad (\psi^*(j+\varsigma+1) - \psi(j+\varsigma) - \hat{z}_2(j)), \ \ j = j_\iota \\ \Lambda(j_{\iota-1}), \ \ j \in (j_{\iota-1}, j_\iota) \end{cases}, \tag{17}$$

$$\begin{cases} \hat{z}(j+\varsigma+1) = \boldsymbol{A}_1 \hat{z}(j+\varsigma) + \hat{\boldsymbol{A}}_2(j)\Delta\Lambda(j) + \\ \qquad \boldsymbol{L}(\psi(j+\varsigma) - \hat{\psi}(j+\varsigma)) \\ \hat{\psi}(j+\varsigma+1) = \boldsymbol{A}_4 \hat{z}(j+\varsigma+1) \end{cases}. \tag{18}$$

5. Convergence analysis

Make an assumption first, before starting the convergence analysis.

Assumption 3 It is assumed that $\Xi(j)$ is nonzero in model (3) and that its sign is fixed, that is, $\Xi(j) \geqslant \delta$ or $\Xi(j) \leqslant -\delta$, in which δ is an algebraically small positive constant.

Remark 7 The rationality of this assumption is that this condition is a linear-like feature of system in (2) that limits the change of control direction. Many model-based control approaches make the assumption that the control direction is known, or at least that its sign is unchanged. The practical implication of this premise is that as the control input rises, the system's output should not decrease. This is not a severe assumption, and this characteristic is not uncommon in many practical industrial systems, such as temperature control systems and pressure control systems.

Give a lemma before the proofs; this lemma will be extremely useful for our results.

Lemma 1 For the iterative format below

$$\boldsymbol{s}(j+1) = \boldsymbol{A}(j)\boldsymbol{s}(j) + \boldsymbol{h}(j), \ \ j = 0, 1, \cdots$$

where $\boldsymbol{A}(j)$ represents a time-varying matrix and $\boldsymbol{h}(j)$ represents a norm bounded vector satisfying $\|\boldsymbol{h}(j)\| \leqslant \varpi$, $\forall j$ with ϖ being the threshold: when the condition $\|\boldsymbol{A}(j)\| \leqslant 1$ is satisfied, the iteration of $\boldsymbol{s}(j+1)$ eventually converges.

The following theorem can be used to summarize DESO-MFAC convergence.

Theorem 1 Consider the non-linear system in (2) satisfying Assumptions 1−3. If the parameters of controller are selected so that

$$\max\left(\left|\frac{2 - l_1 + \sqrt{l_1^2 - 4l_2}}{2}\right|, \left|\frac{2 - l_1 - \sqrt{l_1^2 - 4l_2}}{2}\right|\right) < 1,$$
$$0 < \alpha_1 < 2, \alpha_2 > 0, \eta > 0, \lambda > 0.$$

Applying the proposed DESO-MFAC method (9)−(12) for system to track a constant desired output $\psi^* = \text{const}$, one can guarantee that (i) DESO is iteratively convergent; (ii) for $\forall j$, the estimate of $\hat{\Xi}(j)$ for $\Xi(j)$ is boundedly convergent; (iii) the tracking error $e(j)$ is boundedly convergent.

Proof The proof can be simply divided into three parts. The first part proves the boundedness of each variable of DESO in a finite time; the second part proves the bounded convergence of errors (observer error, tracking

error, and estimation error) in a finite time; and the final part demonstrates that the above convergence could be assured over a sufficiently long period of time.

Part 1 Considering the DESO variable's boundedness, $\psi(j)$, $\hat{\Xi}(j)$, $\hat{z}(j)$, $\Lambda(j)$, and $\xi(j)$ for $j \in \left[0, \tilde{J}\right]$, where $\tilde{J}$ is a finite time

When $j=0$, all of the starting values $|\psi(\varsigma)| < b_{\psi(\varsigma)}$, $\left|\hat{\Xi}(0)\right| < b_{\hat{\Xi}(0)}$, $\|\hat{z}(\varsigma)\| < b_{\hat{z}(\varsigma)}$, $|\Lambda(0)| < b_{\Lambda(0)}$ are all presented in a bounded manner, where $b_{(\cdot)}$ denotes positive constants. Then, according to (2) and (9)−(12), we can get

$$\begin{cases} \psi(\varsigma+1) = g(\boldsymbol{\Psi}(\varsigma), \boldsymbol{\Sigma}(0), \boldsymbol{\Pi}(\varsigma)) \\ \hat{\Xi}(1) = \hat{\Xi}(0) + \dfrac{\alpha_1 \Lambda(0)}{\eta + |\Lambda(0)|^2} \cdot \\ \qquad (\psi(\varsigma+1) - \psi(\varsigma) - \hat{\Xi}(0)\Lambda(0) - \hat{z}_2(0)) \\ \hat{\Xi}(1) = \hat{\Xi}(0),\ \left|\hat{\Xi}(1)\right| \leqslant \varepsilon; \\ \qquad\qquad \text{or } |\Lambda(0)| \leqslant \varepsilon; \\ \qquad\qquad \text{or } \operatorname{sign}(\hat{\Xi}(1)) \neq \operatorname{sign}(\hat{\Xi}(0)) \\ \hat{z}(\varsigma+1) = \boldsymbol{A}_1 \hat{z}(\varsigma) + \hat{\boldsymbol{A}}_2(0)\Lambda(0) + \boldsymbol{L}(\psi(\varsigma) - \hat{z}_1(\varsigma)) \\ \Lambda(1) = \Lambda(0) + \dfrac{\alpha_2 \hat{\Xi}(1)}{\lambda + \left|\hat{\Xi}(1)\right|^2} \cdot \\ \qquad (\psi^*(\varsigma+2) - \psi(\varsigma+1) - \hat{z}_2(1)) \end{cases} \tag{19}$$

Since all parameters on the right-hand side of (19) are bounded, one can obtain that

$$\begin{cases} |\psi(\varsigma+1)| < b_{\psi(\varsigma+1)} \\ \left|\hat{\Xi}(1)\right| < b_{\hat{\Xi}(1)} \\ \|\hat{z}(\varsigma+1)\| < b_{\hat{z}(\varsigma+1)} \\ |\Lambda(1)| < b_{\Lambda(1)} \end{cases}$$

are all bounded too.

In a finite time $j = \tilde{J} > 1$, follow the above steps and continue, we can logically obtain that

$$\begin{cases} \left|\psi(\varsigma+\tilde{J})\right| < b_{\psi(\varsigma+\tilde{J})} \\ \left|\hat{\Xi}(\tilde{J})\right| < b_{\hat{\Xi}(\tilde{J})} \\ \left\|\hat{z}(\varsigma+\tilde{J})\right\| < b_{\hat{z}(\varsigma+\tilde{J})} \\ \left|\Lambda(\tilde{J})\right| < b_{\Lambda(\tilde{J})} \end{cases}$$

are all bounded.

According to the above steps, it is easy to obtain the boundedness of each parameter at time $j = \tilde{J}+1$. As a result, we can deduce from mathematical induction that

$$\begin{cases} \max\limits_{j\in[0,\tilde{J}]} |\psi(\varsigma+j)| < b_\psi \\ \max\limits_{j\in[0,\tilde{J}]} \left|\hat{\Xi}(j)\right| < b_{\hat{\Xi}} \\ \max\limits_{j\in[0,\tilde{J}]} \|\hat{z}(\varsigma+j)\| < b_{\hat{z}} \\ \max\limits_{j\in[0,\tilde{J}]} |\Lambda(j)| < b_\Lambda \end{cases}$$

are all bounded.

On the basis of the definition of ξ in (3), the boundedness of $\max\limits_{j\in[0,\tilde{J}]} |\xi(j)| < b_\xi$ can be guaranteed by the boundedness of $\max\limits_{j\in[0,\tilde{J}]} |\psi(\varsigma+j)| < b_\psi$, $\max\limits_{j\in[0,\tilde{J}]} |\Lambda(j)| < b_\Lambda$ and $\left|\sup \Pi(j)\right| \leqslant b_\pi$.

Part 2 The tracking error's bounded convergence, and the convergence of parameter estimation error, for $j \in \left[0, \tilde{J}\right]$

(i) Defining the observer error as

$$\tilde{z}(j+\varsigma) = z(j+\varsigma) - \hat{z}(j+\varsigma) = \left[\tilde{z}_1(j+\varsigma), \tilde{z}_2(j)\right]^{\mathrm{T}}.$$

The dynamic equation of the observer error can be obtained by (7) and (8):

$$\begin{aligned} \tilde{z}(j+\varsigma+1) = (\boldsymbol{A}_1 - \boldsymbol{L}\boldsymbol{A}_4)\tilde{z}(j+\varsigma) + \\ \boldsymbol{A}_3 \omega(j) + (\boldsymbol{A}_2(j) - \hat{\boldsymbol{A}}_2(j))\Delta\Lambda(j). \end{aligned} \tag{20}$$

Since the boundedness of $\psi(j)$, $\hat{\Xi}(j)$, $\hat{z}(j)$, $\Lambda(j)$, and $\xi(j)$ has already been shown above, in the iterative equation in (20), according to Lemma 1, we can get that $\tilde{z}(j+\varsigma)$ is iteratively convergent with increased time by making the spectral radius of matrix $\|\boldsymbol{A}_1 - \boldsymbol{L}\boldsymbol{A}_4\| \leqslant 1$. We can select the parameter of the observer gain $\boldsymbol{L}$ to be

$$\max\left(\left|\frac{2 - l_1 + \sqrt{l_1^2 - 4l_2}}{2}\right|, \left|\frac{2 - l_1 - \sqrt{l_1^2 - 4l_2}}{2}\right|\right) < 1$$

to meet the above requirements for the matrix spectrum radius.

(ii) The tracking error $e(j)$ can be expressed as

$$e(j+\varsigma) = \psi^* - \psi(j+\varsigma)$$

and by the system in (3) and the control law in (6), the error expression is shown as follows:

$$\begin{aligned} e(j+\varsigma+1) = e(j+\varsigma)\left(1 - \frac{\alpha_2 \Xi(j)\hat{\Xi}(j)}{\lambda + \left|\hat{\Xi}(j)\right|^2}\right) + \\ \frac{\alpha_2 \Xi(j)\hat{\Xi}(j)}{\lambda + \left|\hat{\Xi}(j)\right|^2} \hat{z}_2(j) - \xi(j). \end{aligned}$$

Taking the absolute value of both sides of the equation gives the following formula:

$$\begin{aligned} |e(j+\varsigma+1)| \leqslant |e(j+\varsigma)| \left|\left(1 - \frac{\alpha_2 \Xi(j)\hat{\Xi}(j)}{\lambda + \left|\hat{\Xi}(j)\right|^2}\right)\right| + \\ \left|\frac{\alpha_2 \Xi(j)\hat{\Xi}(j)}{\lambda + \left|\hat{\Xi}(j)\right|^2}\right| |\hat{z}_2(j)| + |\xi(j)|. \end{aligned} \tag{21}$$

According to Assumption 2 and the resetting algorithm (11) for the initial value of $\hat{\Xi}(0)$, one can obtain that the signs of $\Xi(j)$ and $\hat{\Xi}(j)$ are the same, that is $\Xi(j)\hat{\Xi}(j) \geqslant \delta\varepsilon > 0$.

Selecting appropriate α_2 and λ such that

$$0 < \frac{\alpha_2 \delta\varepsilon}{\lambda + b_{\hat{z}}{}^2} \leqslant \frac{\alpha_2 \Xi(j)\hat{\Xi}(j)}{\lambda + \left|\hat{\Xi}(j)\right|^2} \leqslant \frac{\alpha_2 L_{n_\psi+2}\left|\hat{\Xi}(j)\right|}{2\sqrt{\lambda}\left|\hat{\Xi}(j)\right|} = \frac{\alpha_2 L_{n_\psi+2}}{2\sqrt{\lambda}} < 1. \tag{22}$$

So there exists $0 < d_1 < 1$ such that

$$0 < (1 - \frac{\alpha_2 \Xi(j)\hat{\Xi}(j)}{\lambda + \left|\hat{\Xi}(j)\right|^2}) \leqslant d_1 < 1. \tag{23}$$

Substitute (22) and (23) into (21), and combine the boundedness of $\hat{z}_2(j)$ and $\xi(j)$ in a finite time. Assume $\max\limits_{j\in[0,\bar{J}]}|\hat{z}_2(j)| \leqslant b_{\hat{z}_2}$, $b_{\hat{z}_2}$ is a positive constant. One can obtain

$$|e(j+\varsigma+1)| \leqslant d_1|e(j+\varsigma)| + \frac{\alpha_2 L_{n_\psi+2}}{2\sqrt{\lambda}} b_{\hat{z}_2} + b_\xi,$$

further

$$|e(j+\varsigma+1)| \leqslant d_1^{j+1}|e(\varsigma)| + \frac{1-d_1^{j+1}}{1-d_1}\chi_1 \tag{24}$$

where $\chi_1 = \dfrac{\alpha_2 L_{n_\psi+2}}{2\sqrt{\lambda}} b_{\hat{z}_2} + b_\xi$.

Inequation in (24) indicates a bounded convergence of tracking error in finite time since the beginning value $e(\varsigma)$ is bounded.

(iii) When $|\Delta\Lambda(j-1)| \leqslant \varepsilon$, according to the resetting algorithm in (11), $\hat{\Xi}(j) = \hat{\Xi}(0)$ may be obtained, ensuring the boundedness of $\hat{\Xi}(j)$.

When $|\Delta\Lambda(j-1)| > \varepsilon$, using the system in (3) and parameter estimation law (4), we have

$$\tilde{\Xi}(j) = \tilde{\Xi}(j-1)\left(1 - \frac{\alpha_1|\Delta\Lambda(j-1)|^2}{\eta + |\Delta\Lambda(j-1)|^2}\right) + \frac{\alpha_1|\Delta\Lambda(j-1)|}{\eta + |\Delta\Lambda(j-1)|^2}\hat{z}_2(j-1) - \frac{\alpha_1|\Delta\Lambda(j-1)|}{\eta + |\Delta\Lambda(j-1)|^2}\xi(j-1) + \Xi(j) - \Xi(j-1)$$

where $\tilde{\Xi}(j) = \Xi(j) - \hat{\Xi}(j)$.

Taking both sides of the equation's absolute value

$$|\tilde{\Xi}(j)| \leqslant |\tilde{\Xi}(j-1)|\left|\left(1 - \frac{\alpha_1|\Delta\Lambda(j-1)|^2}{\eta + |\Delta\Lambda(j-1)|^2}\right)\right| + \left|\frac{\alpha_1\Delta\Lambda(j-1)}{\eta + |\Delta\Lambda(j-1)|^2}\right||\hat{z}_2(j-1)| + \left|\frac{\alpha_1\Delta\Lambda(j-1)}{\eta + |\Delta\Lambda(j-1)|^2}\right||\xi(j-1)| + |\Xi(j) - \Xi(j-1)|. \tag{25}$$

Since $0 < \alpha_1 < 2$ and $\eta > 0$, there exists $0 < d_2 < 1$ so that

$$0 < (1 - \frac{\alpha_1|\Delta\Lambda(j-1)|^2}{\eta + |\Delta\Lambda(j-1)|^2}) \leqslant d_2 < 1, \tag{26}$$

and

$$0 < \frac{\alpha_1\Delta\Lambda(j-1)}{\eta + |\Delta\Lambda(j-1)|^2} \leqslant \frac{\alpha_1}{2\sqrt{\eta}}. \tag{27}$$

Since the boundedness of $\hat{z}_2(j)$ and $\xi(j)$ in a finite time have been proven, substituting (26) and (27) into (25), we can get

$$|\tilde{\Xi}(j)| \leqslant d_2|\tilde{\Xi}(j-1)| + \frac{\alpha_1}{2\sqrt{\eta}}b_{\hat{z}_2} + \frac{\alpha_1}{2\sqrt{\eta}}b_\xi + 2L_{n_\psi+2}.$$

Represent $|\tilde{\Xi}(j-1)|$ in the same form as above as

$$|\tilde{\Xi}(j-1)| \leqslant d_2|\tilde{\Xi}(j-2)| + \frac{\alpha_1}{2\sqrt{\eta}}b_{\hat{z}_2} + \frac{\alpha_1}{2\sqrt{\eta}}b_\xi + 2L_{n_\psi+2}.$$

Substituting in we get

$$|\tilde{\Xi}(j)| \leqslant d_2^2|\tilde{\Xi}(j-2)| + d_2(\frac{\alpha_1}{2\sqrt{\eta}}b_{\hat{z}_2} + \frac{\alpha_1}{2\sqrt{\eta}}b_\xi + 2L_{n_\psi+2}) + \frac{\alpha_1}{2\sqrt{\eta}}b_{\hat{z}_2} + \frac{\alpha_1}{2\sqrt{\eta}}b_\xi + 2L_{n_\psi+2}.$$

Continue the above steps to get

$$\begin{aligned}|\tilde{\Xi}(j)| &\leqslant d_2^2|\tilde{\Xi}(j-2)| + d_2(\frac{\alpha_1}{2\sqrt{\eta}}b_{\hat{z}_2} + \frac{\alpha_1}{2\sqrt{\eta}}b_\xi + 2L_{n_\psi+2}) + \frac{\alpha_1}{2\sqrt{\eta}}b_{\hat{z}_2} + \frac{\alpha_1}{2\sqrt{\eta}}b_\xi + 2L_{n_\psi+2} \leqslant \\ &d_2^3|\tilde{\Xi}(j-3)| + d_2^2(\frac{\alpha_1}{2\sqrt{\eta}}b_{\hat{z}_2} + \frac{\alpha_1}{2\sqrt{\eta}}b_\xi + 2L_{n_\psi+2}) + d_2(\frac{\alpha_1}{2\sqrt{\eta}}b_{\hat{z}_2} + \frac{\alpha_1}{2\sqrt{\eta}}b_\xi + 2L_{n_\psi+2}) + \\ &\frac{\alpha_1}{2\sqrt{\eta}}b_{\hat{z}_2} + \frac{\alpha_1}{2\sqrt{\eta}}b_\xi + 2L_{n_\psi+2}\cdots \leqslant \\ &d_2^j|\tilde{\Xi}(0)| + \frac{1-d_2^j}{1-d_2}(\frac{\alpha_1}{2\sqrt{\eta}}b_{\hat{z}_2} + \frac{\alpha_1}{2\sqrt{\eta}}b_\xi + 2L_{n_\psi+2}).\end{aligned}$$

The last item is obtained according to the summation formula of the proportional series.

Let

$$\chi_2 = \frac{\alpha_1}{2\sqrt{\eta}}b_{\hat{z}_2} + \frac{\alpha_1}{2\sqrt{\eta}}b_\xi + 2L_{n_\psi+2},$$

and we can get

$$|\tilde{\Xi}(j)| \leqslant d_2^j|\tilde{\Xi}(0)| + \frac{1-d_2^j}{1-d_2}\chi_2. \tag{28}$$

Since the initial value $\tilde{\Xi}(0)$ is bounded, (28) implies a bounded convergence of $\tilde{\Xi}(j)$ in a finite time. Moreover, the boundedness of $\hat{\Xi}(j)$ is obvious because of the boundedness of $\Xi(j)$.

Part 3 The tracking error convergence for $\forall j$

In Part 1 and Part 2, The DESO variables $\psi(j)$, $\hat{\Xi}(j)$,

$\hat{z}(j)$, $\Lambda(j)$, and $\xi(j)$ have all been proven to be bounded, and the constrained convergence of tracking error has been assured $\forall j \in [0, \tilde{J}]$. We can get $\psi(\tilde{J}+1)$, $\hat{\Xi}(\tilde{J}+1)$, $\hat{z}(\tilde{J}+1)$, $\Lambda(\tilde{J}+1)$, and $\xi(\tilde{J}+1)$ if we continue to follow (9)−(12). Then we may deduce that $\psi(j)$, $\hat{\Xi}(j)$, $\hat{z}(j)$, $\Lambda(j)$, and $\xi(j)$ are all bounded for $\forall j$. Therefore, the bounded convergence of $e(j)$ and $\tilde{\Xi}(j)$ can been guaranteed for $\forall j$. In addition, assuming $\sup|\hat{z}_2(j)| \leqslant b_{\hat{z}_2}$ and $\sup|\xi(j)| < b_\xi$, according to (24) and (28) we can conclude that $\lim\limits_{j\to\infty} e(j) \leqslant \dfrac{\chi_1}{1-d_1}$ and $\lim\limits_{j\to\infty} \tilde{\Xi}(j) \leqslant \dfrac{\chi_2}{1-d_2}$, for $0 < d_1 < 1$, $0 < d_2 < 1$. □

The following theorem is presented to assure the asymptotic convergence of the system's tracking error after introducing the event-triggered mechanism.

Theorem 2 Take a nonlinear system in (2) that meets Assumptions 1−3. The suggested ET-DESO-MFAC algorithms (14)−(18) can ensure that the tracking error $e(j)$ converges asymptotically with increasing time with correct controller parameter selection.

Proof The tracking error is re-expressed as follows using the system model in (3):

$$e(j+\varsigma+1) = \psi^*(j+\varsigma+1) - \psi(j+\varsigma) - \Xi(j)\Delta\Lambda(j) - \xi(j). \tag{29}$$

According to the control law in (17), at the triggered instants, i.e., $j = j_\iota$, (29) becomes

$$\begin{aligned} e(j+\varsigma+1) &= \psi^*(j+\varsigma+1) - \psi(j+\varsigma) - \\ &\Xi(j)(\Lambda(j_\iota) - \Lambda(j_{\iota-1})) - \xi(j) = \\ &(1-\Xi(j)H(j))(\psi^*(j+\varsigma+1) - \\ &\psi(j+\varsigma) - \hat{z}_2(j)). \end{aligned}$$

The Lyapunov function is chosen as follows:

$$V(j) = e^2(j).$$

Then one has

$$\begin{aligned} \Delta V(j+\varsigma+1) &= e^2(j+\varsigma+1) - e^2(j+\varsigma) = \\ &[(1-\Xi(j)H(j))(\psi^*(j+\varsigma+1) - \\ &\psi(j+\varsigma) - \hat{z}_2(j))]^2 - e^2(j+\varsigma). \end{aligned} \tag{30}$$

Because the event-triggered error is $\sigma(j) = e(j_\iota) - e(j)$, it is evident that at the event-triggered moment, $\sigma(j_\iota) = 0$. We can reach the following result by combining this conclusion with the event-triggered condition in (13).

$$\frac{\kappa(j+\varsigma)}{2\Xi^2(j)H^2(j)} \geqslant 0 \tag{31}$$

Since the denominator of inequation in (31) is a square term, the following conclusion can be drawn:

$$\begin{aligned} \kappa(j+\varsigma) &= e^2(j+\varsigma) - 4[(1-\Xi(j)H(j))\cdot \\ &(\psi^*(j+\varsigma+1) - \psi(j+\varsigma) - \hat{z}_2(j))]^2 \geqslant 0. \end{aligned} \tag{32}$$

According to (30) and (32), it is easy to get

$$\Delta V(j+\varsigma+1) \leqslant 0.$$

□

This finding implies that the ET-DESO-MFAC approach, as conceived, may cause the tracking error to converge asymptotically at all event-triggered moments.

The control input inside this time frame stays precisely the same as the input at the previous trigger instant during the event interval, i.e., $j \in (j_\iota - 1, j_\iota)$. When the input remains constant, the system's properties are obviously stable.

6. Coordinate compensation algorithm

When tracking a SV' trajectory, a desired trajectory will be given in advance. Assume that the desired trajectory's coordinate at time j is $(x^*(j), y^*(j))$ and that the desired yaw angle is $\psi^*(j)$. $\psi^*(j)$ can be calculated according to the following formula:

$$\begin{cases} \Delta x^*(j+1) = x^*(j+1) - x^*(j) \\ \Delta y^*(j+1) = y^*(j+1) - y^*(j) \\ \psi^*(j+1) = \arctan(\dfrac{\Delta y^*(j+1)}{\Delta x^*(j+1)}) \end{cases}.$$

However, at the initial movement, there is a tracking error between the actual yaw angle $\psi(j)$ and the desired yaw angle $\psi^*(j)$. Even in the subsequent control process, the actual angle can track the desired angle well, there may be a steady-state error between the desired trajectory $(x^*(j), y^*(j))$ and the actual trajectory $(x(j), y(j))$. Therefore, the desired yaw angle $\psi^*(j+1)$ needs to be compensated according to the current position, the desired position at the next moment, and the desired yaw angle at the next moment.

The principle of coordinate compensation is shown in Fig. 3. In Fig. 3, EF is the given desired trajectory, and the vessel departs from E to F. $p(j)$ and $p^*(j+1)$ respectively represent the current position of the vessel and the desired position at the next moment. $\bar{\psi}(j)$ and $\psi^*(j+1)$ respectively represent the direction angle of $p(j) \to p^*(j+1)$ and the desired angle at the next moment. And the arc $Ep(j)$ represents the actual trajectory of the vessel. Obviously, the actual position $p(j)$ of the vessel has deviated from the desired trajectory.

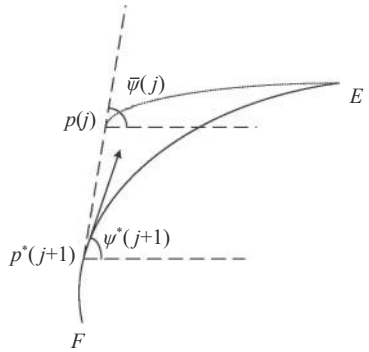

Fig. 3 Principle of desired angle compensation

If the above deviation occurs in the trajectory while tracking the desired angle, the desired angle $\psi^*(j+1)$ must be corrected so that the corrected desired angle contains the position error information of the vessel, thereby eliminating the trajectory tracking error while tracking the desired angle.

The compensation algorithm is as follows:

$$\tilde{\psi}^*(j+1) = \psi^*(j+1) + \beta(\varphi(j) - \psi^*(j+1))$$

where β denotes compensation coefficient that adjust the compensation intensity, $\tilde{\psi}^*(j+1)$ denotes the desired yaw angle after compensation, and

$$\varphi(j) = \arctan\left(\frac{y(j) - y^*(j+1)}{x(j) - x^*(j+1)}\right).$$

The algorithm with coordinate compensation is as follows:

$$\tilde{\psi}^*(j+\varsigma+1) = \psi^*(j+\varsigma+1) + \beta(\varphi(j+\varsigma) - \psi^*(j+\varsigma+1)), \tag{33}$$

$$\hat{\Xi}(j) = \hat{\Xi}(j-1) + \frac{\alpha_1 \Delta\Lambda(j-1)}{\eta + |\Delta\Lambda(j-1)|^2} \cdot (\Delta\psi(j+\varsigma) - \hat{\Xi}(j-1)\Delta\Lambda(j-1) - \hat{z}_2(j-1)), \tag{34}$$

$$\hat{\Xi}(j) = \hat{\Xi}(0),\ |\hat{\Xi}(j)| \leqslant \varepsilon;\ \text{or } |\Delta\Lambda(j-1)| \leqslant \varepsilon;\ \text{or } \operatorname{sign}(\hat{\Xi}(j)) \neq \operatorname{sign}(\hat{\Xi}(0)), \tag{35}$$

$$j = j_\iota, \quad \sigma^2(j+\varsigma) > \frac{\kappa(j+\varsigma)}{2\Xi^2(j)H^2(j)}, \tag{36}$$

$$\Lambda(j) = \begin{cases} \Lambda(j_{\iota-1}) + \dfrac{\alpha_2 \hat{\Xi}(j)}{\lambda + |\hat{\Xi}(j)|^2} \cdot (\psi^*(j+\varsigma+1) - \psi(j+\varsigma) - \hat{z}_2(j)), & j = j_\iota \\ \Lambda(j_{\iota-1}), & j \in (j_{\iota-1}, j_\iota) \end{cases}, \tag{37}$$

$$\begin{cases} \hat{z}(j+\varsigma+1) = \boldsymbol{A}_1 \hat{z}(j+\varsigma) + \hat{\boldsymbol{A}}_2(j)\Delta\Lambda(j) + \boldsymbol{L}(\psi(j+\varsigma) - \hat{\psi}(j+\varsigma)) \\ \hat{\psi}(j+\varsigma+1) = \boldsymbol{A}_4 \hat{z}(j+\varsigma+1) \end{cases}. \tag{38}$$

The block diagram of DESO-MFAC control system with coordinate compensation is shown in Fig. 4.

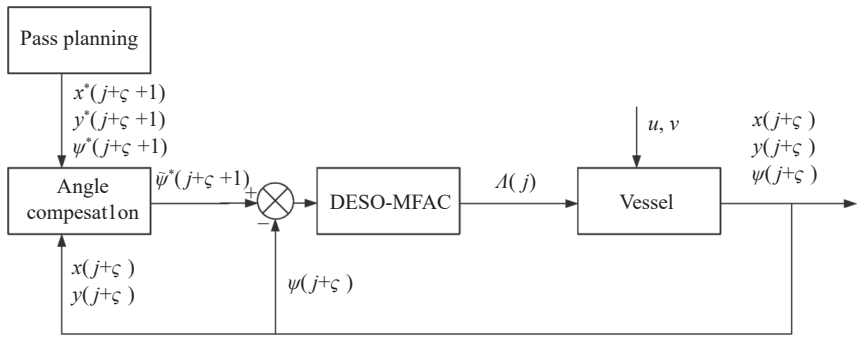

Fig. 4 Block diagram of DESO-MFAC control system with coordinate compensation

The real-time position of the vessel can be obtained by the inertial navigation method using the data collected by the gyroscope and the photoelectric encoder. The vessel's target angle compensation algorithm gives the corrected target angle at the next moment according to the current position, the target position at the next moment and the target angle at the next moment. The ET-DESO-MFAC controller corrects the control input according to the difference between the corrected target angle and the current angle.

7. Simulation results

To further validate the effectiveness of the suggested approach, it is simulated as follows.

The simulation research consists of five parts: (i) angle tracking error; (ii) trajectory tracking; (iii) event-triggered points; (iv) change of control law; (v) error of DESO. The initial position coordinates and initial angle of the SV are respectively set as $(x(0), y(0)) = (0, 0)$ and $\psi(\varsigma+1) = \psi(\varsigma) = \pi/4$. Set the fixed velocities of the SV u = 1.3 m/s, v = 0 m/s. Set initial value $\xi(0) = 0$ and

$\Lambda(0)=0$. And set the time delay $\varsigma=0.05$ s, disturbance $\pi(j)=0.1\sin(j/10)$.

The parameter settings of the algorithm in (33)−(38) are shown in Table 1.

Table 1 Time of different algorithms

Parameter	Value
$\hat{\Xi}(0)$	1.0
α_1	0.1
η	0.1
α_2	0.992
λ	0.1
ε	0.1×10^{-10}
l_1	0.8
l_2	0.2
β	0.01

(i) Angle tracking error (e_ψ)

The simulation result of angle tracking error based on ET-DESO-MFAC method with coordinate compensation is shown in Fig. 5.

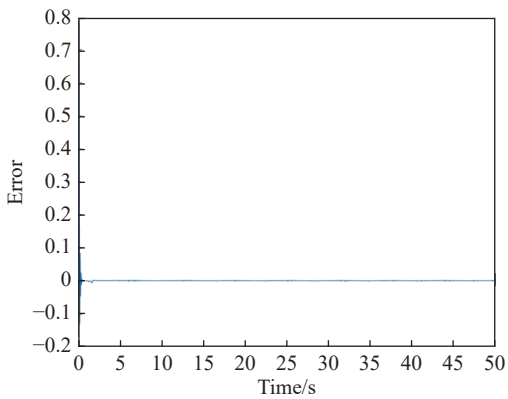

Fig. 5 Angle tracking error of ET-DESO-MFAC method with coordinate compensation

According to Fig. 5, angle tracking error of ET-DESO-MFAC method with coordinate compensation can converge to zero. More importantly, the convergence speed is quite fast, so the proposed method performs well in practical applications. The control signal of the ET-DESO-MFAC control method is not updated all the time, but it can control the tracking error within a certain range.

(ii) Trajectory tracking

Before studying the trajectory tracking of the SV, firstly, set a desired trajectory as $y=\sin x$. Then, the initial algorithm and the algorithm with coordinate compensation are respectively used to control the SV to track the ideal trajectory.

The simulation result of trajectory tracking based on ET-DESO-MFAC method with coordinate compensation is shown in Fig. 6.

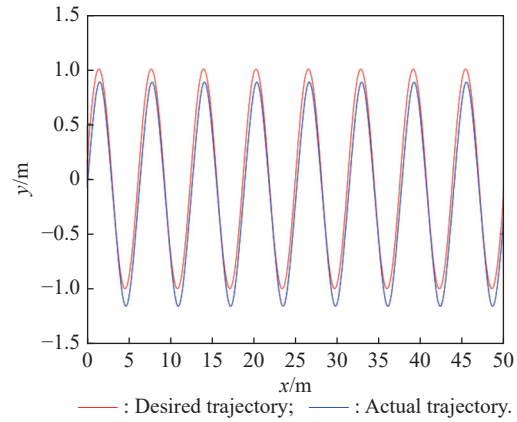

Fig. 6 Trajectory tracking of ET-DESO-MFAC method with coordinate compensation

From Fig. 6, we can see that the SV under the control of ET-DESO-MFAC method with coordinate compensation has a good tracking effect on the desired trajectory $y=\sin x$.

For an SV system with external disturbances, Fig. 7 is the trajectory tracking diagram obtained by the DESO-MFAC method in [36]. The DESO-MFAC method updates the control law at every moment and achieves good results. However, this method is not suitable for some situations, such as the environment with limited communication bandwidth, and the situation of sensor and signal transmission delay. In addition, the DESO-MACD method does not consider the coordinate information of SVs when implementing trajectory tracking.

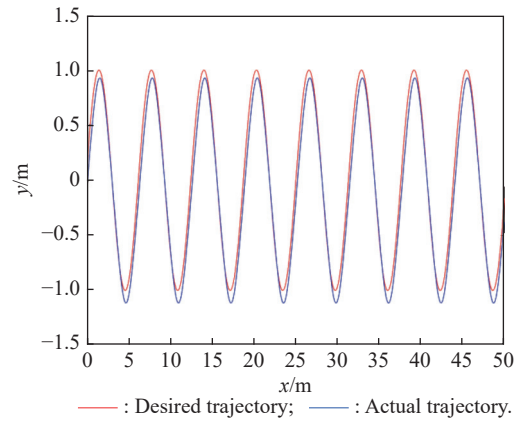

Fig. 7 Trajectory tracking of DESO-MFAC method

Compared with the original method, Fig. 6 is the trajectory tracking diagram obtained by using our proposed algorithm. As can be seen from the figure, there is a certain lag between the actual trajectory and the ideal trajec-

tory due to the time delay we added to the original system. In addition, our proposed algorithm updates the control law only when the tracking error is greater than a preset threshold, which is beneficial for use in a bandwidth-limited environment. And we also incorporate the coordinate information of the SV into the control algorithm. In conclusion, our proposed improved method has a broader application background.

(iii) Event-triggered points

In Fig. 8, the red points represent the event-triggered points, that is, the time points when the control input signals are updated.

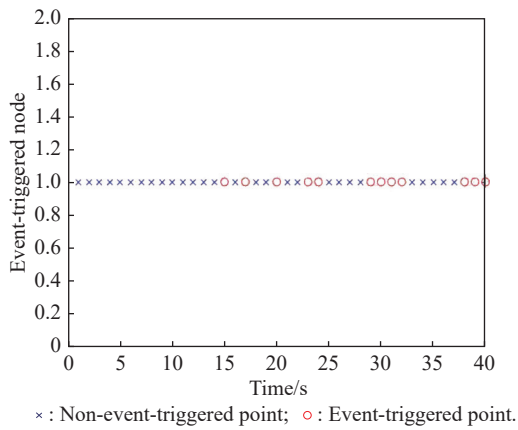

Fig. 8 Event-triggered points

(iv) Change of control law ($\Lambda(j)$)

The change of control law based on ET-DESO-MFAC method with coordinate compensation is shown in Fig. 9.

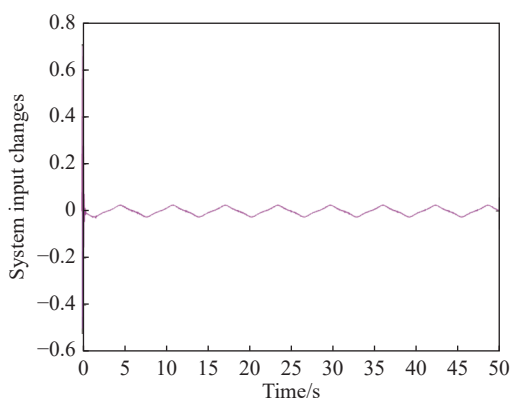

Fig. 9 Change of control law

The associated control law varies substantially since the SV must be managed to follow the correct trajectory from the beginning location in the first few seconds, as seen in the figure. The SV reaches the preset trajectory after a few seconds, and the control law fluctuations grow smaller and more regular.

(v) Error of DESO (e_{z_2})

In this paper, the DESO method is used to estimate $\xi(j)$. Next, we conduct a simulation analysis on the convergence of DESO.

According to Fig. 10, the estimation error can be controlled within a certain range.

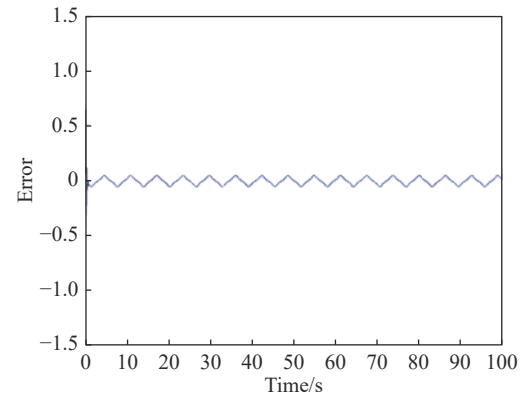

Fig. 10 DESO error

8. Conclusions

Aiming at the problem of vessel trajectory tracking with time delay, bounded disturbance and limited bandwidth, this paper proposes ET-DESO-MFAC method with coordinate compensation to provide a practical solution. Firstly, the proposed method only uses the input and output data of the vessel system and does not contain any model information. Second, ETC is based on event-triggered condition, which lowers data transmission throughout the control process. Then, the target angle is rectified online using the coordinate compensation technique, reducing the steady-state inaccuracy of the proposed controller even more. Followed by, the convergence of DESO-MFAC is proved by mathematical methods, and the convergence of ET-DESO-MFAC is guaranteed by using the Lyapunov function. Finally, the simulation results demonstrate that the suggested technique has a high tracking accuracy.

References

[1] NAEEM W, XU T, TIANO A. The design of a navigation, guidance, and control system for an unmanned surface vehicle for environmental monitoring. Proceedings of the Institution of Mechanical Engineers Part M Journal of Engineering for the Maritime Environment, 2008, 222(2): 67–79.

[2] CACCIA M, BIBULI M, BONO R, et al. Unmanned surface vehicle for coastal and protected waters applications: the charlie project. Marine Technology Society Journal, 2007, 41(2): 62–71.

[3] PRABHU T. Unmanned surface vehicle(USV) for coastal surveillance. International Journal of Mechanical Engineering and Technology, 2016, 7: 13–28.

[4] WANG J H, GU W, ZHU J X, et al. An unmanned surface

vehicle for multi-mission applications. Proc. of the International Conference on Electronic Computer Technology, 2009: 358−361.

[5] QIAO L, ZHANG W D. Adaptive non-singular integral terminal sliding mode tracking control for autonomous underwater vehicles. IET Control Theory & Applications, 2017, 11(8): 1293–1306.

[6] CHEN H, ZHANG B W, ZHAO T B, et al. Finite-time tracking control for extended nonholonomic chained-form systems with parametric uncertainty and external disturbance. Journal of Vibration and Control, 2018, 24(1): 100–109.

[7] CHEN H. Robust stabilization for a class of dynamic feedback uncertain nonholonomic mobile robots with input saturation. International Journal of Control Automation & Systems, 2014, 12(6): 1216–1224.

[8] XU J, WANG M, QIAO L. Dynamical sliding mode control for the trajectory tracking of underactuated unmanned underwater vehicles. Ocean Engineering, 2015, 105: 54–63.

[9] LI X D, LI P. Stability of time-delay systems with impulsive control involving stabilizing delays. Automatica, 2020, 124: 109336.

[10] YUAN J X, QIU Z, WANG F X. Sliding mode observer controller design for a two-dimensional aeroelastic system with gust load. Asian Journal of Control, 2019, 21(1): 130–142.

[11] AN H, FIDAN B, WU Q Q. Sliding mode differentiator based tracking control of uncertain nonlinear systems with application to hypersonic flight. Asian Journal of Control, 2019, 21(1): 143–155.

[12] LIU Y C, ZHU Q D. Adaptive fuzzy control for ship autopilot with course constraint based on event-triggered mechanism. Proc. of the 7th International Conference on Information, Cybernetics, and Computational Social Systems, 2020: 175−179.

[13] DU J L, GUO C, YU S H, et al. Adaptive autopilot design of time-varying uncertain ships with completely unknown control coefficient. IEEE Journal of Oceanic Engineering, 2007, 32(2): 346–352.

[14] VELAGIC J, VUKIC Z, OMERDIC E. Adaptive fuzzy ship autopilot for track-keeping. Control Engineering Practice, 2003, 11(4): 433–443.

[15] DIMAROGONAS D, FRAZZOLI E, JOHANSSON K. Distributed event-triggered control for multi-agent systems. IEEE Trans. on Automatic Control, 2012, 57(5): 1291–1297.

[16] LI S, AHN C K, GUO J, et al. Neural-network approximation-based adaptive periodic event-triggered output-feedback control of switched nonlinear systems. IEEE Trans. on Cybernetics, 2021, 51(8): 4011–4020.

[17] LI M, LI S, AHN C K, et al. Adaptive fuzzy event-triggered command-filtered control for nonlinear time-delay systems. IEEE Trans. on Fuzzy Systems, 2022, 30(4): 1025–1035.

[18] SUN Y J, LIU Y, TIAN X C. Realization of coordinate compensation algorithm in numerical control for steel grating flame cutting system. Proc. of the Chinese Automation Congress, 2017: 2266−2270.

[19] MA Y H, LI Y, JIANG L, et al. A compensation algorithm of tool path for grinding wheel wear in solid cutting tool flank grinding. Proceedings of the Institution of Mechanical Engineers, Part B: Journal of Engineering Manufacture, 2022, 236(3): 245–254.

[20] HOU Z S, DONG H R, JIN S T. Model-free adaptive control with coordinates compensation for automatic car parking systems. Acta Automatica Sinica, 2015, 41(4): 823–831.

[21] GRABMAIR G, MAYR S, HOCHWALLNER M, et al. Model based control design-a free tool-chain. Proc. of the European Control Conference, 2014: 826 −831.

[22] GAN M G, ZHANG M, MA H X, et al. Adaptive control of a servo system based on multiple models. Asian Journal of Control, 2016, 18(2): 652–663.

[23] WANG Y, WEI X Z, ZHANG H. Dynamic event-based control of nonlinear stochastic systems. IEEE Trans. on Automatic Control, 2017, 62(12): 6544–6551.

[24] LIU Y, BU R X, GAO X R. Ship trajectory tracking control system design based on sliding mode control algorithm. Polish Maritime Research, 2018, 25(3): 26–34.

[25] SHEN Z P, ZHANG X L, ZHANG N, et al. Recursive sliding mode dynamic surface output feedback control for ship trajectory tracking based on neural network observer. Control Theory and Applications, 2018, 35(8): 1092–1100.

[26] HOU Z S. On model-free adaptive control: the state of the art and perspective. Control Theory and Applications, 2006, 23(4): 586–592.

[27] HOU Z S, JIN S T. Data-driven model-free adaptive control for a class of mimo nonlinear discrete-time systems. IEEE Trans. on Neural Networks, 2011, 22(12): 2173.

[28] HOU Z S, WANG Z. From model-based control to data-driven control: survey, classification and perspective. Information Sciences, 2013, 235: 3–35.

[29] CAO Z Q, CAO R M, HOU Z S, et al. Multiple input multiple output model free adaptive contour control for two-dimensional linear motor. Control Theory and Applications, 2020, 37(5): 1007–1017. (in Chinese)

[30] GAO H, MA G F, GUO Y N, et al. Data-driven model-free adaptive attitude control of partially constrained combined spacecraft with external disturbances and input saturation. Chinese Journal of Aeronautics, 2019, 32(5): 1281–1293.

[31] WANG J H, TAN G X, SUN C M. Research on vehicle four-wheel steering based on model-free adaptive control. Proc. of the 5th International Conference on Electromechanical Control Technology and Transportation, 2020: 372−376.

[32] YAO W L, LIU Y, ZHANG J D, et al. Ship electrical propulsion control system based on improved model-free adaptive control. Proc. of the 26th Chinese Control and Decision Conference, 2014: 1526−1529.

[33] TUTSOY O, BARKANA D E. Model free adaptive control of the under-actuated robot manipulator with the chaotic dynamics. ISA Transactions, 2021, 118: 106–115.

[34] HUANG Y, WANG J Z, SHI D W, et al. Performance assessment of discrete-time extended state observers: theoretical and experimental results. IEEE Trans. on Circuits and Systems I: Regular Papers, 2018, 65(7): 2256–2268.

[35] CHI R H, HUI Y, ZHANG S H, et al. Discrete-time extended state observer-based model-free adaptive control via local dynamic linearization. IEEE Trans. on Industrial Electronics, 2020, 67(10): 8691–8701.

[36] HOU M D, WANG Y S. Data-driven trajectory tracking sliding mode constraint control for wheeled mobile robot. Control and Decision, 2020, 35(6): 1353–1360.

[37] FOSSEN T. Guidance and control of ocean vehicle. New York: John Wiley & Sons, 1994.

[38] ZHOU P, ZHANG S, WEN L, et al. Kalman filter-based data-

driven robust model-free adaptive predictive control of a complicated industrial process. IEEE Trans. on Automation Science and Engineering, 2022, 19(2): 788–803.

[39] DONG N, LYU W J, ZHU S, et al. Anti-noise model-free adaptive control and its application in the circulating fluidized bed boiler. Proceedings of the Institution of Mechanical Engineers, Part I: Journal of Systems and Control Engineering, 2021, 235(8): 1472–1481.

[40] HOU Z S, JIN S T. Model free adaptive control: theory and applications. New York: John Wiley & Sons, 2013.

Biographies

CHEN Hua was born in 1978. He received his B.S. degree from the Department of Mathematics at Yangzhou University, China, in 2001, M.S. degree from the Department of Management Sciences and Engineering, Nanjing University, China, in 2009, and Ph.D. degree from the Department of Control Science and Engineering, University of Shanghai for Science and Technology, China, in 2012. He is a researcher at the College of Science, Hohai University. His main research interests include modelling and control of nonlinear systems, stability analysis, time delay systems, and motion control of underactuated systems such as wheeled mobile robots, unmanned surface vehicle, and inspection robots.
E-mail: chenhua112@163.com

SHEN Chao was born in 1999. He received his B.S. degree from the School of Mathematical Science, Huaiyin Normal University, China, in 2017. He is currently pursuing his M.S. degree at the College of Science, Hohai University, China. His research interests include data-driven control, control of discrete systems and control of surface vessels.
E-mail: 1277220206@qq.com

HUANG Jiahui was born in 1999. She received her B.S. degree from the Department of Mathematics, Huaiyin Normal University, China, in 2021. She is currently pursuing her M.S. degree at the College of Science, Hohai University. Her research interests include data-driven control and time-delay control of wheeled mobile robots.
E-mail: 1353988290@qq.com

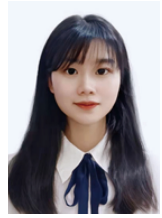

CAO Yuhan was born in 2001. Currently, she is a undergraduate student at Hohai-Lille College, Hohai University. Her main research interests include modelling and control of nonlinear systems, stability analysis, time-delay-systems, motion control of underactuated systems such as unmanned surface vehicle.
E-mail: 1371615921@qq.com